Residue R120 Is Essential for the Quaternary Structure and Functional Integrity of Human αB-Crystallin†

Stéphanie Simon,*,‡ Magalie Michiel,§ Fériel Skouri-Panet,|| Jean Pierre Lechaire,⊥ Patrick Vicart,‡ and Annette Tardieu§

EA 300, Université Paris 7, Case 7136, 75251 Paris Cedex 05, France, FRE2852, CNRS-Université Paris 6, case 29, 7 quai St Bernard, 75252 Paris Cedex 05, France, UMR7590, CNRS-IPGP-Universités Paris 6 et 7, 140 rue de Lourmel, 75015 Paris, France, and Service de Microscopie Electronique IFR 83, Université Paris 6, case 25, 7 quai St Bernard, 75252 Paris cedex 05, France

Received February 14, 2007; Revised Manuscript Received May 22, 2007

ABSTRACT: The missense mutation Arg-120 to Gly (R120G) in the human αB-crystallin sequence has been reported to be associated with autosomal dominant myopathy, cardiomyopathy, and cataract. Previous studies of the mutant showed a significant ability to aggregate in cultured cells and an increased oligomeric size coupled to an important loss of the chaperone-like activity *in vitro*. The aim of this study was to further analyze the role of the R120 residue in the structural and functional properties of αB-crystallin. The following mutants were generated, Arg-120 to Gly (R120G), Cys (R120C), Lys (R120K), and Asp (R120D). *In cellulo*, after expression in two cultured cell lines, NIH-3T3 and Cos-7, the capacity of the wild-type and mutant crystallins to aggregate was evaluated and the protein location was determined by immunofluorescence. *In vitro*, the wild-type and mutant crystallins were expressed in *Escherichia coli* cells, purified by size exclusion chromatography, and characterized using dynamic light scattering, electron microscopy, and chaperone-like activity assays. Aggregate sizes *in cellulo* and *in vitro* were analyzed. The whole of the data showed that the preservation of an Arg residue at position 120 of αB-crystallin is critical for the structural and functional integrity of the protein and that each mutation results in specific changes in both structural and functional characteristics.

The α-crystallins belong to the small heat shock protein (sHSP)[1] family (*1*). The sHSPs are found in most organisms (archea, bacteria, plants, and animals) where they are generally induced in response to a variety of physiological and environmental stress (*2*, *3*). In humans, 10 sHSPs have been identified (*4*, *5*). Whereas αA-crystallin (αA) is essentially expressed in lens, αB-crystallin (αB) is also expressed in other tissues (muscle, heart, lung, etc.), where it is often found to be associated with other sHSPs (*6*, *7*). A number of point mutations leading to pathologies have now been identified (*8*). The most well-known is the mutation of Arg-120 to Gly in αB (R120G), which is responsible for an autosomal dominant myopathy associated with cardiomyopathy and cataract (*9*). The R120 residue seems particularly interesting. The corresponding mutation in αA (R116C) causes congenital cataract (*10*) and in HSP22 (K141E or K141N) is responsible for distal hereditary motor neuropathy and Charcot Marie Tooth disease (*11*, *12*). In all these inherited diseases, the transmission is autosomal dominant. Moreover, the equivalent mutation in HSP27 (R148G) induces accumulation of aggregates in cells (*13*). The involvement of this conserved residue in inherited human diseases highlights its important role in the structure and function of sHSPs.

The sHSP family is characterized by a highly conserved C-terminal domain of ∼90 amino acids, "the α-crystallin domain" (*14*), and a variable N-terminal domain. A typical feature of sHSPs is the formation of large oligomeric complexes (12−40 subunits of 12−50 kDa). In plants and archae, sHSPs have a fixed number of subunits, whereas in mammals, they are polydisperse. In mammalian lenses, αA and αB associate in a 3/1 ratio to form polydisperse oligomers of ∼40 ± 5 subunits and of 800 kDa (*15*), whereas αA and αB alone form polydisperse oligomers smaller in size, ∼30 subunits and 600 kDa (*16*). So far, only three three-dimensional (3D) structures of sHSPs are known, one from a hyperthermophile archae *Methanoccus jannaschii*, HSP16.5, with 24 subunits (*17*); one from wheat, *Triticum aestivum*, HSP16.9, with 12 subunits (*18*); and one from a parasitic flatworm, *Taenia saginata*, Tsp36, with two subunits, each subunit containing two α-crystallin domains (*19*). A fourth

† This work was supported by the French Ministry of Research (S.S. and M.M.), by the Association Française contre les Myopathies (AFM) (S.S. and Grant 11764 to P.V.), by University Paris 7 (P.V.), by University Paris 6 (F.S.-P. and A.T.), and by the Centre National de la Recherche Scientifique (CNRS) (F.S.-P. and A.T.).

* To whom correspondence should be addressed: EA 300, Université Paris 7, Case 7136, 75251 Paris Cedex 05, France. Phone: 33 1 44 27 47 36. Fax: 33 1 44 27 36 11. E-mail: stef.labo@gmail.com.

‡ EA 300, Université Paris 7.

§ FRE2852, CNRS-Université Paris 6.

|| UMR7590, CNRS-IPGP-Universités Paris 6 et 7.

⊥ IFR83, Université Paris 6.

[1] Abbreviations: WT, wild-type; SDS−PAGE, sodium dodecyl sulfate−polyacrylamide gel electrophoresis; ADH, alcohol dehydrogenase; CS, citrate synthase; DLS, dynamic light scattering; αA and αB, αA- and αB-crystallin, respectively; hαB-WT, human wild-type αB-crystallin; sHSP, small heat shock protein; PBS, phosphate-buffered saline; 3D, three-dimensional.

10.1021/bi7003125 CCC: $37.00
Published on Web 07/27/2007

one is in progress, from the bacteria *Xanthomonas axonopodis* pv. citri (*20*), whereas the multiple assemblies of a fifth one, HSP26 from the yeast *Saccharomyces cerevisiae*, have been modeled from cryoelectron microscopy, yet at a lower resolution (*21*). Sequence comparison coupled with structure analysis revealed that the R120 mutation was located on a highly conserved β-strand (*19*).

The α-crystallins share unique physicochemical properties, including the ability to rapidly exchange their subunits while keeping the same average number of subunits (*22*, *23*). Moreover, they can change their size and oligomeric state with the *in vitro* environment (pH, temperature, etc.) through subunit exchange (*24*). Both *in vivo* and *in vitro* they function as molecular chaperones (*9*, *25*−*31*), whose main function is to associate, not refold, a variety of stress-denatured proteins and prevent further aggregation, in an ATP-independent process. Subunit exchange might control the chaperone-like activity, often associated with changes in oligomeric state (*32*).

The α-crystallins therefore exhibit structural and functional properties in the living world that seem closely associated with their dynamic structure, yet the process by which a point mutation may be sufficient to modify these properties and lead to pathologies remains to be determined. To address these questions, we constructed and expressed in different systems several position 120 αB mutants: R120G, R120C, R120K, and R120D. The *in cellulo* and *in vitro* properties of wild-type (WT) and mutant crystallins were analyzed. After expression in cultured cell lines, the capacity to aggregate of the WT and mutant crystallins was evaluated and the protein location was determined by immunofluorescence. The soluble assemblies were characterized *in vitro* by dynamic light scattering, electron microscopy, and chaperone assays.

EXPERIMENTAL PROCEDURES

Cloning and Site-Directed Mutagenesis. Cloning of the hαB-WT and R120G cDNA into the pcDNA3 vector (Invitrogen) has been reported previously for the *in cellulo* studies (*9*). The R120C, R120D, and R120K mutants were generated by site-directed mutagenesis. For the *in vitro* studies, each mutant DNA was then subcloned into bacterial expression vector pET16b (Novagen); the hαB-WT cDNA used for expression in *E. coli* was kindly provided by W. W. de Jong (*33*) and was cloned into vector pET24d (Novagen). Detailed cloning information and primers used are given in Table 1. All the recombinant vectors were sequenced by automated sequencing.

Cell Culture, Transfection, and Immunofluorescence. Two different cell lines, adherent and easy to transfect, were chosen. The murine NIH-3T3 cells are devoid of sHSP expression in the absence of stress. The monkey Cos-7 cells are devoid of αB expression but express HSP27 constitutively. The cells were grown in DMEM Glutamax medium (Gibco), supplemented with 10% fetal calf serum (FCS, Gibco) and penicillin/streptomycin (Gibco) in a 5% CO_2 humidified atmosphere. One day prior to transfection, cultured cells were trypsinized and plated on glass coverslips placed in a culture dish. Transfection with 3 μg of each pcDNA3 recombinant vector was carried out using Fugene 6 (Roche Diagnostics) according to the manufacturer's instructions; 24 or 48 h later, cells were rinsed twice with phosphate-buffered saline (PBS) before being fixed and permeabilized by incubation in a cold methanol/acetone solution (7/3) for 5 min at 4 °C. After several washes in PBS, cells were probed using monoclonal mouse antibody anti-αB (1/200, Stressgen) diluted in PBS containing 2% FCS. The primary antibody was then detected using a goat anti-mouse antibody coupled to Alexa Fluor 11031 (1/1000, Molecular Probes) diluted in PBS and 2% FCS. The samples were mounted on coverslips using Mowiol (Sigma). Cells were examined using a fluorescence microscope (LEITZ) and images collected via an ORCA-ER digital camera (Hamamatsu) and processed using Simple PCI 6.0 (Compix Inc. imaging systems).

Table 1: Detailed Information about the Used Constructs

construct number	construct designation	method of cloning/ source of the cDNA	restriction site used	primers[a]
1	pcDNA3-αB WT	described previously[b]	KpnI/XbaI	−
2	pcDNA3-αB R120G	described previously[b]	KpnI/XbaI	−
3	pcDNA3-αB R120C	site-directed mutagenesis	KpnI/XbaI	a, b, c, d
4	pcDNA3-αB R120D	site-directed mutagenesis	KpnI/XbaI	a, b, e, f
5	pcDNA3-αB R120K	site-directed mutagenesis	KpnI/XbaI	a, b, g, h
6	pET24d-αB WT	described previously[c]	XhoI/EcoRI	−
7	pET16b-αB R120G	subcloning from 2	NcoI/XhoI	−
8	pET16b-αB R120C	subcloning from 3	NcoI/XhoI	−
9	pET16b-αB R120D	subcloning from 4	NcoI/XhoI	−
10	pET16b-αB R120K	subcloning from 5	NcoI/XhoI	−

[a] a, 5′-aaaaaaggtaccatggacatcgccatccaccac-3′; b, 5′-aaaaaatcta-gactatttcttgggggctgcggt-3′; c, cagggagttccactgc aaataccggatccca; d, 5′-tgggatccggtatttgcagtggaactccctg-3′; e, 5′-tccagggagttccacgataaatac-cggatccc-3′; f, 5′-gggatccggtatttatcgtggaactccctgga-3′; g, 5′-tccagggagttccacaaaaaatacggatccc-3′; h, 5′-gggatccggtatttttttgtggaac tccctgg-3′. [b] From ref *9*. [c] From ref *33*.

To test the expression level of each transfected construct, cells were lysed 48 h post-transfection in buffer A [125 mM Tris-HCl (pH 6.8), 4% SDS, 20% glycerol, 400 mM dithiothreitol, and 0.01% bromophenol blue] prior to the analysis by Western blotting using the monoclonal mouse anti-αB-crystallin antibody (1/10000, Stressgen). A monoclonal mouse anti-vimentin antibody (1/2000, DakoCytomation) was used to normalize the amount of total protein loaded.

Assessment of the Ability of hαB-WT and Mutants To Aggregate in Cell Cultures. The presence or absence of aggregates in transitory transfected cells was scored for, at least, 100 randomly transfected cells for each construct. Each datum is the mean value of three independent experiments ± the standard error. A one-way ANOVA test was applied to compare results between sample groups. Differences between groups were considered statistically significant if the p value was <0.05.

Expression and Purification of hαB-WT and Mutants. αB-Crystallins were expressed in *E. coli* strain BL21(DE3) and induced with 0.1 mM isopropyl α-D-thiogalactoside (IPTG) for 3.5 h at 37 °C. After disruption of the cell wall using the "Bug Buster master mix" (Novagen) completed with 0.2 μM AEBSF (Novagen), which is an irreversible inhibitor of serine proteases, and 100 mM NaCl, the soluble protein fraction was dialyzed against buffer B [22 mM Na_2HPO_4, 28 mM KH_2PO_4, 70 mM KCl, 1.3 mM EDTA, 3 mM NaN_3, and 3 mM DTT (pH 6.8)] with 0.6 mM phenylmethane-

sulfonyl fluoride (PMSF). The next step was a nucleic acid precipitation with 0.12% poly(ethyleneimine) (PEI). Finally, hαB-WT and mutants were purified by gel filtration FPLC. According to the culture volume, chromatography was conducted either on a S200PG column or on a S200HR column (Amersham Bioscience) and eluted in buffer B. The identity was controlled by mass spectrometry (MS/MS). The purity of the αB preparations was assessed by 12% SDS−PAGE, colored with Coomassie blue. Purified proteins were stocked at 4 °C and never freeze-dried.

Dynamic Light Scattering (DLS) Measurements of R_h and Polydispersity. DLS measurements were performed on a DynaPro from Wyatt Technology Corp. (formerly Protein Solutions) using regularization methods (software, Dynamics, version 6). With this equipment, the laser light wavelength is 830 nm and the scattered light is collected at 90° by an optic fiber until a detector is reached. The sample cell can be thermostated with a Peltier element, from 4 to 80 °C. As macromolecules are subjected to Brownian motions, their relative positions change as a function of time in a size-dependent manner. With monodisperse solutions of particles, the measurement of the autocorrelation function of the scattered light as a function of time allows us to determine the diffusion coefficient of the species in solution, D_T. The hydrodynamic radius, R_h, is then calculated from the Stokes−Einstein equation, in which $R_h = K_B T/6\pi D_T \eta$, where K_B is the Boltzman constant, T the absolute temperature, and η the viscosity of the solvent. With globular particles and assuming a level of hydration of ∼25%, the MW can be estimated using the equation $MW = {}^4/_3\pi N_a(R_h)^3$.

With a monomodal distribution of polydisperse particles, an average hydrodynamic radius is obtained and the percentage of polydispersity is calculated in addition. These values are calculated with DynaProDYNAMICS. When several species are present in solution, the number of species can be determined, as well as the average hydrodynamic radius and the polydispersity of each species, yet the accuracy is better when only two or three clearly different species are present. The technique was used to measure the hαB-WT and mutant size and polydispersity at 20 and 48 °C and to check the stability of these values as a function of time. All the samples were filtered before experiments on Nanosep MF GHP, 0.45 μm centrifugation devices to eliminate large aggregates or dust particles. The protein concentration was 0.1−1 mg/mL, the sample volume 50 μL, the acquisition time for one measurement 10 s, and the laser power sensitivity 50%. Each experiment consisted of 15−360 measurements.

Assay for the Determination of Chaperone-like Activity of hαB-WT and Its Mutants with Alcohol Dehydrogenase (ADH). The capacity of hαB-WT and different mutants to prevent 1,10-phenanthroline-induced ADH (Sigma) denaturation and aggregation was determined. The assay was conducted at 42 °C in 500 μL reaction volumes in buffer C [50 mM sodium phosphate buffer (pH 7.2) and 100 mM NaCl] containing ADH at 0.4 mg/mL in the presence or absence of hαB-WT or mutants at 0.08 mg/mL (i.e., 5/1 ADH/αB ratio). The assay was monitored for 40 min at 360 nm on a UVIKON 923 spectrometer. Control experiments were conducted with hαB-WT and mutants alone under the same conditions.

Assay for the Determination of Chaperone-like Activity of hαB-WT and Its Mutants with Citrate Synthase (CS). The chaperone activity was assayed with DLS, by monitoring as a function of time the light scattered at 90° by the sample. Indeed, measuring the scattered intensity at 90° in DLS equipment is equivalent to measuring the scattered intensity in a spectrometer (although the wavelengths are different) and can be used to monitor heat-induced aggregation. Most CS assays reported in the literature have been performed between 37 and 45 °C (e.g., ref *48*), yet a rapid DLS analysis of CS aggregation as a function of temperature demonstrated a faster process at 48 °C. The chaperone assay was therefore conducted at 48 °C so that it could be more significant. The scattering of the CS alone and of the CS in the presence of hαB-WT or mutants was first measured at 20 °C in a separate experiment and shown to remain constant as a function of time. Then, after equilibration at 48 °C of the DynaPro, the sample cell was placed in the sample holder and the scattered intensity was recorded as a function of time over 0.5 or 1 h periods. To optimize the signal, the CS and αB concentrations were ∼2.2 and ∼0.5 mg/mL, respectively (i.e., a CS/αB ratio of 4.5/1). Control experiments were carried out with hαB-WT and mutants alone under the same conditions; i.e., the scattered intensities were first recorded at 20 °C and then monitored for 1 h at 48 °C. After 1 h at 48 °C, the hαB-WT scattering had increased by ∼10% and the R120G scattering by ∼25%. The values of the other mutants were between those. Eighty microliter reaction volumes were used in buffer B. The laser power sensitivity was 50%, and the acquisition time for one measurement was 10 s. Each experiment therefore consisted of 180 or 360 measurements.

Energy-Filtered Transmission Electron Microscopy (EFTEM). Negative staining was carried out at 20 °C using carbon-coated grids. A sample drop at ∼1 mg/mL was deposited on the grid and negatively stained with a 2% aqueous uranyl acetate solution. The specimens were examined with a LEO 912 (ZEISS 120 kV) "in-column" energy spectrometer (Omega filter) transmission electron microscope.

RESULTS

Location and Characterization of hαB-WT and Mutant Assemblies in Mammalian Cell Lines. The immunofluorescence location of hαB-WT and the different mutants was determined 24 and 48 h after transfection in Cos-7 and NIH-3T3 cells. These cell lines were chosen since NIH-3T3 cells do not have endogenous sHSPs, whereas Cos-7 cells express a high level of endogenous HSP27 associated with a low level of αB. The different αB-crystallin species presented the same type of location in the two transfected cell lines (Figure 1). As expected from previous work (*9*), hαB-WT exhibited a diffuse cytoplasmic pattern at both 24 and 48 h (Figure 1A,B,K,L). Instead, 24 h after transfection, the R120G mutant was found essentially as well-defined multifocus-like aggregates in the cytoplasm (Figure 1E,O); 48 h after transfection, the R120G-induced aggregates were bigger and perinuclear (Figure 1F,P). The location of the R120G mutant at 24 and 48 h is in agreement with previously published studies (*9*, *34*). The mutant R120K exhibited the same pattern of distribution as hαB-WT (Figure 1C,D,M,N). The mutants R120C (Figure 1G,H,Q,R) and R120D (Figure 1I,J,S,T) had a tendency to form aggregates and a location similar to those of R120G 24 h after transfection. Note that

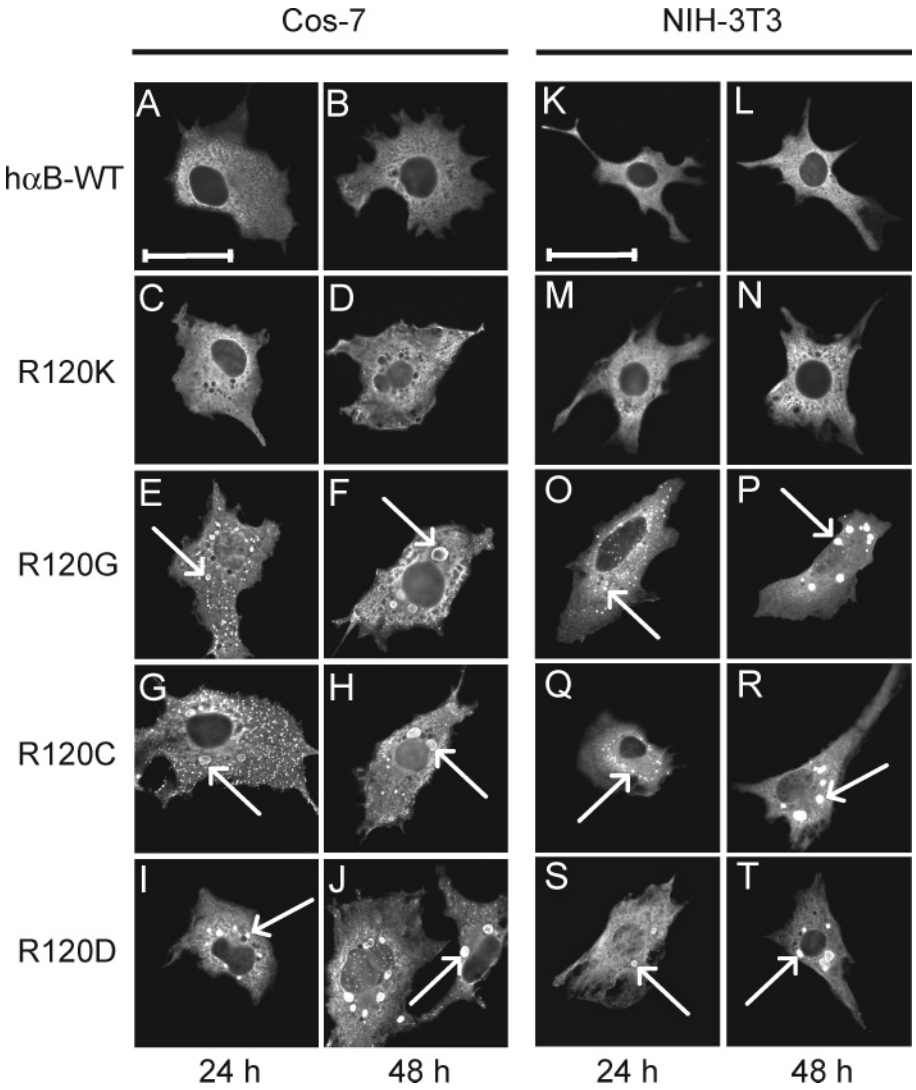

FIGURE 1: Cellular location of hαB-WT, R120K, R120G, R120C, and R120D in Cos-7 and NIH-3T3 cells 24 and 48 h post-transfection. hαB-WT (A, B, K, and L) and R120K (C, D, M, and N) show a diffuse immunostaining within the cytoplasm in both cell lines 24 and 48 h after transfection. In contrast, the expression of R120G (E, F, O, and P), R120C (G, H, Q, and R), and R120D (I, J, S, and T) induced the formation of cytoplasmic and/or perinuclear aggregates that can be observed 24 h after transfection in both cell lines. Arrows indicate the presence of aggregates in cells. The scale bar is 50 μm.

the R120D aggregates seemed even bigger than those of R120G. At 48 h, however, large aggregates were also observed for R120C and R120G which can be seen in Figure 1. The presence of hαB-WT and mutants species in the nucleus was observed only in a small, nonsignificant number of cells, which can be seen in Figure 1E,J,O,P.

Aggregation Kinetics in Mammalian Cell Lines. As the ability to aggregate is a time-dependent phenomenon (*34*), we determined the percentage of transfected cells containing aggregates 24 and 48 h after transfection in Cos-7 and NIH-3T3 cells. Figure 2A shows the results obtained 24 h after transfection in Cos-7 cells. No aggregates could be observed with hαB-WT and R120K, with a background of <1%. Instead, the R120G, R120C, and R120D mutants exhibited a significant tendency to form aggregates with 20.2 ± 1.4, 23.9 ± 2.1, and 18.2 ± 1.4% of transfected cells, respectively, containing aggregates, i.e., no significant difference among these three mutants. The same observations were established in NIH-3T3 cells (data not shown); 48 h post-transfection (Figure 2B), the background of aggregation of hαB-WT, 2.0 ± 1.0%, and R120K, 3.0 ± 1.7%, did not show significant variation, whereas the R120D mutant and, moreso, the R120G and R120C mutants showed an increased number of transfected cells with aggregates with 34.0 ± 2.6, 35.7 ± 3.9, and 20.0 ± 5.2%, respectively. The same results were obtained in NIH-3T3 cells (data not shown). Figure 2C shows the variation of the number of aggregates in transfected cells as a function of time. It can be seen on the figure that the increase in the number of transfected cells with aggregates for the R120G and R120C mutants was more important than for the R120D mutant, suggesting that, in Cos-7 cells, R120G and R120C mutants aggregate quicker than R120D. The level of synthesized protein was determined to be similar in all the transfected constructs, eliminating the possibility of a dose-dependent effect. The analysis was done by Western blotting, with a specific antibody against αB, on the total protein extracts of the transfected cells, 48 h post-transfection (data not shown).

Expression and Solubility in the Bacterial Host. We previously observed with native bovine α-crystallin that renaturation procedures after, for example, dissociation in urea yielded particles with a lower molecular mass. We

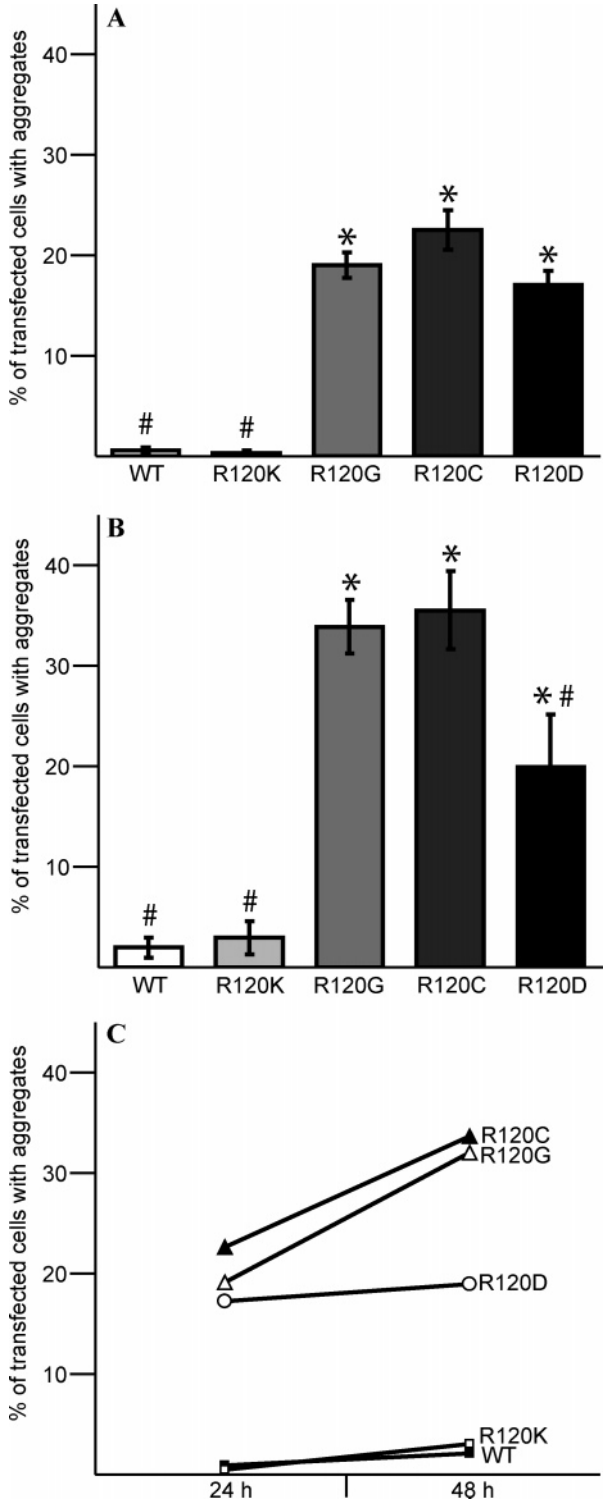

FIGURE 2: Capacity of hαB-WT and R120K, R120G, R120C, and R120D mutants to aggregate in Cos-7 cells 24 and 48 h after transfection. Percentage of transfected cells containing aggregates (A) 24 and (B) 48 h after transfection in Cos-7 cells. Each histogram represents the mean of three independent experiments. The bar indicates the standard error. The data between groups were analyzed using a one-way ANOVA. Differences between groups were considered statistically significant if p was <0.05. An asterisk indicates groups significantly different from the hαB-WT and R120K groups. A number sign indicates groups significantly different from the hαB-R120G and R120C groups. (C) Representation of aggregate formation as a function of time in Cos-7 cells. Note that the number of transfected cells containing aggregates increases slowly for hαB-WT, R120K, and R120D and rapidly for R120G and R120C.

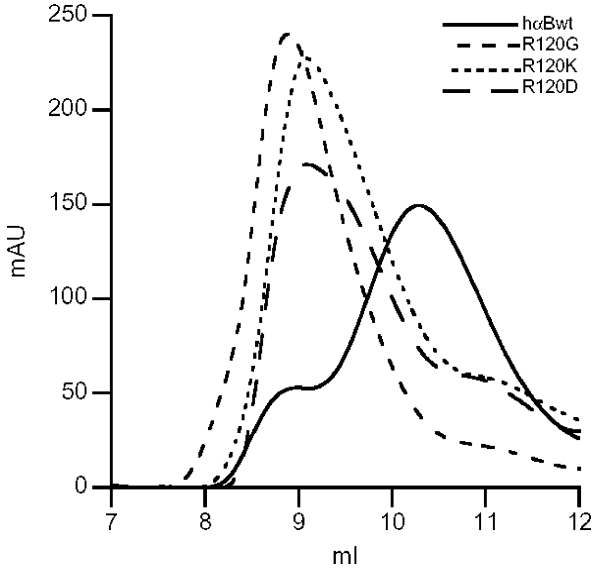

FIGURE 3: Gel filtration chromatography of hαB-WT, R120K, R120G, or R120D mutant performed on a S200HR column. The flow rate was 0.75 mL/min. Fractions of 0.25 mL were collected and checked via SDS gels. Only one band was observed for hαB-WT. With the mutants eluting close to the void volume, and especially with the R120G mutant, a few minor bands, barely detectable, could be observed in addition.

therefore did not want to resolubilize inclusion bodies to avoid any possible change in the "native" oligomeric state and looked for expression conditions in *E. coli* that are able to provide us with sufficient protein in the soluble fraction. Under our optimal conditions, hαB-WT and the mutant R120K were mainly found in the bacterial soluble fraction whereas a significant fraction of the R120G and R120D mutants remained in the insoluble one. The R120C mutant was found exclusively in the insoluble fraction (data not shown).

Purification and Characterization by Gel Filtration of Recombinant Assemblies. Soluble total extracts of proteins were purified by gel filtration via FPLC. Since only the soluble fraction was used for the final purification, the mutant R120C could not be purified. The yield for hαB-WT and for the mutants was, on average, between 2 and 5 mg for a 100 mL culture. Typical elution profiles are shown in Figure 3. hαB-WT eluted as a sharp symmetrical peak at a position corresponding approximately to 600−680 kDa (sometimes, a few aggregates were eluting in the void volume). All the other mutants eluted close to or in the void volume, indicating a mass of >1000 kDa. The molecular mass was increasing in the following order: WT < R120K ≤ R120D < R120G. For the mutants, a shoulder was often observed in the elution profile, corresponding to a lower molecular mass of ∼500 kDa. For subsequent analyses, only the main peak was considered. For all mutants, and especially for R120G, the crystallin yield was shown to be higher and the FPLC profile more reproducible when FPLC was performed immediately after the preparation of the total protein extracts. Therefore, in the experiments presented here, small culture volumes were used and the purification was conducted with an S200 HR column to proceed with all the purification steps on the same day.

Stability in Vitro. Once purified, hαB-WT was stable for several weeks; i.e., both the solubility and the particle size

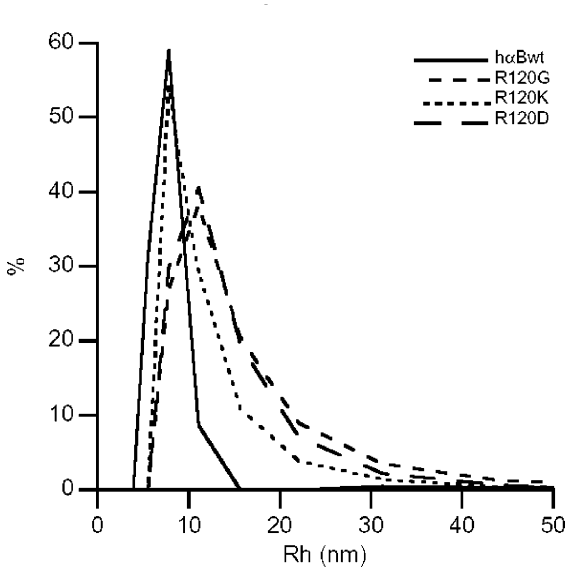

FIGURE 4: Best-fit distribution of the R_h values calculated by the DLS instrument for each sample. The measurements were taken at 20 °C immediately after purification. The acquisition time was 10 s and the laser power sensitivity 50%. The sample concentration was 0.4 mg/mL. Each experiment was an average of at least 15−360 measurements.

Table 2: Summary of the Data[a]

	charge on residue 120	*in vitro* stability	R_h (nm)	polydispersity (%)	protection of ADH (%)	protection of CS (%)
hαB-WT	+1	++	7.6	17.0	99	97
R120K	+1	+	10.9	46.1	21	84
R120G	0	− −	13.3	58.2	0	61
R120D	−1	−	12.8	48.5	0	77

[a] The average R_h and polydispersity values correspond to the preparations shown in Figure 4 and dynamic light scattering conducted at 20 °C. For the chaperone assays, the percentages of protection toward ADH and CS were calculated from Figures 6 and 7 at $t = {}^1/_2$. Stability refers to the ability of proteins to remain in solution as a function of time.

remained essentially unchanged. On the other hand, the R120G mutant exhibited a strong tendency to precipitate as a function of time, with most of the material already precipitated in a few days. R120K and R120D had intermediate behaviors: R120K increased slightly in size in a week or so, whereas R120D rapidly increased in size in a few days; both mutants formed a few percent of precipitates at the same time (data not shown). This result led us to conduct the DLS and chaperone assay measurements shortly after the purification procedure.

Determination of Hydrodynamic Radii and Polydispersity with DLS. The *in vitro* size, shape, and polydispersity of hαB-WT and R120 mutants were investigated at 20 °C with DLS. One series of preparations is shown in Figure 3, and the corresponding best-fit distribution of R_h values and polydispersities are shown in Figure 4. The numerical values are given in Table 2. As we can see in Figure 4, the distribution profiles were rather different for hαB-WT and for the mutants. Moreover, the profiles observed with the mutants were asymmetrical, indicating the presence of a significant fraction of particles with large sizes and molecular masses. The R_h values at the maximum of the distribution were found to increase in the following order: hαB-WT ≤ R120K < R120D ≈ R120G. The width of the distribution

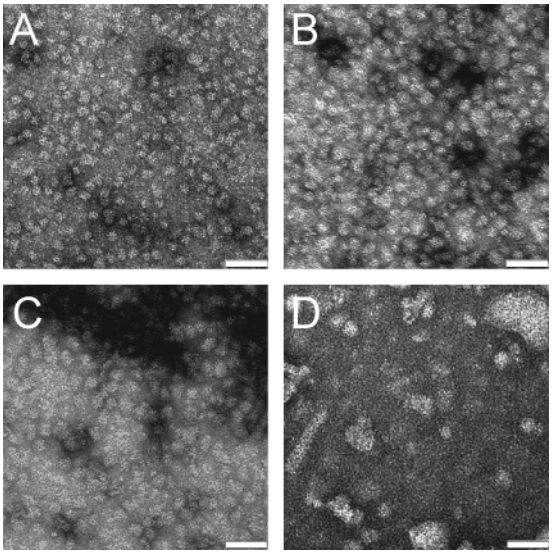

FIGURE 5: Transmission electron micrographs of the αB samples negatively stained with 2% uranyl acetate and photographed at a magnification of 50000×. The solid bar represents 50 nm for all micrographs: (A) hαB-WT, (B) R120K mutant, (C) R120G mutant, and (D) R120D. Note that the particle size and polydispersity increase from panel A to D.

was increasing in the following order: hαB-WT < R120K < R120D ≤ R120G. These data are representative of the results obtained with different preparations (∼10) over a period of 1 year. Indeed, the values obtained for hαB-WT were reproducibly found to be 7.6 ± 0.3 nm with a percentage of polydispersity of <20%. When analyzed on the same day, the hydrodynamic radii of R120G were also reproducibly found to be ∼13.3 nm, yet the polydispersity was much higher, on the order of 58%, with a significant part of the particles having hydrodynamic radii of >30−50 nm. Moreover, over a period of a few days, the sample had precipitated in part and the R_h value of the remaining soluble fraction had increased. Instead, the values found for the R120K mutant were much more variable from one preparation to the other, e.g., between 11 and 15 nm up to 20 nm in one case; however, the polydispersity remained generally limited to ∼40%, and the observed values were stable with time. The R120D values were both varying with the preparation and increasing as a function of time with, in all cases, a high percentage of polydispersity, ∼50%. When analyzed as a function of temperature, the hαB-WT and the R120 mutants were found to be remarkably stable until 50 °C with only small variations in hydrodynamic radius and polydispersity.

Visualization of Size and Polydispersity with EFTEM. The electron microscopy studies were consistent with the DLS data. On the EM fields, hαB-WT appeared homogeneous in size with, on average, an external diameter of 15 ± 2 nm. An example is given in Figure 5A. All the mutants were bigger and more polydisperse, as shown in Figure 5B−D. The polydispersity particularly increased for the R120G (Figure 5C) and R120D (Figure 5D) mutants, where the presence of a significant number of large particles with a variety of shapes, from quasi-spherical up to elongated ones, was clearly visible. However, since the electron microscopy could not always be performed immediately after the preparation, part of these aggregates could also originate from some aging of the preparation.

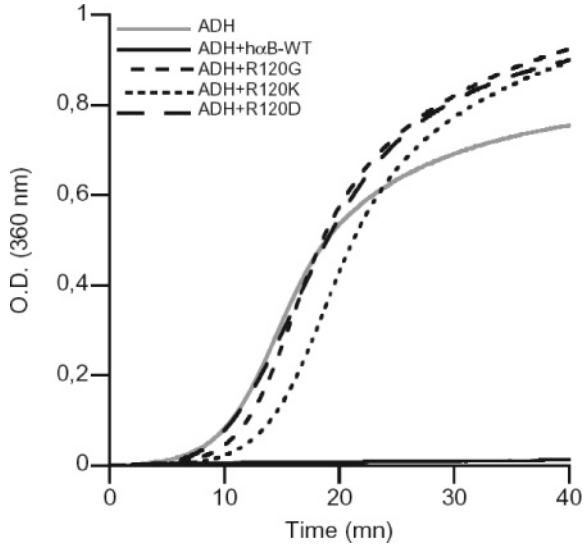

FIGURE 6: Chaperone-like activity of the αB samples toward ADH. Optic density at 360 nm was measured as a function of time at 42 °C. Each plot corresponds to the mean of two independent experiments. hαB-WT protected ADH against aggregation and/or precipitation, whereas R120K, R120G, and R120D mutants do not. Note that the aggregation and/or precipitation of ADH in the presence of the R120K mutant is delayed compared to the aggregation and/or precipitation of ADH in the presence of R120G or R120D. The ADH/αB ratio was 5/1.

Chaperone-like Activity in Vitro. The chaperone-like activity of hαB-WT and of the mutants was investigated using two target proteins, ADH and CS. In the ADH assays, the experiments were conducted with at least two different protein preparations and were repeated, in each case, at least three times. The assay was carried out at 42 °C, using an ADH/αB ratio of 5/1. As one can see in Figure 6, hαB-WT was able to prevent 90−100% of the aggregation of ADH by 1,10-phenanthroline at 42 °C. In contrast, the R120G, R120D, and R120K mutants had no effect at all on the aggregation of ADH, indicating that all the mutants had lost the *in vitro* chaperone-like activity. Note, however, that CS aggregation and/or precipitation started later for the R120K mutant than for the other mutants.

The CS assay was adapted for DLS experiments, as indicated in Experimental Procedures. The scattered intensities recorded at 48 °C with CS incubated alone or in the presence of hαB-WT or mutants (using a CS/αB ratio of 4.5/1) are shown in Figure 7. The curves were subtracted for the values recorded at 20° to be directly comparable with the curves in Figure 6. The percentages of protection calculated at 30 min from Figure 7 are given in Table 2. As one can see from Table 2 and Figure 7, hαB-WT was able to prevent CS aggregation. The chaperone-like activity of the mutants was found to decrease with an increase in size and polydispersity, yet all the mutants retained a significant chaperone-like activity toward CS. The results were reproducible from one preparation to another. After some days, however, the chaperone ability of the mutants, and especially that of the R120G, was reduced, whereas that of hαB-WT remained stable (data not shown).

Taken together, the results obtained with the ADH and CS assays demonstrate a target protein specificity of the mutants and a direct connection between chaperone-like activity and mutant quaternary structure and stability.

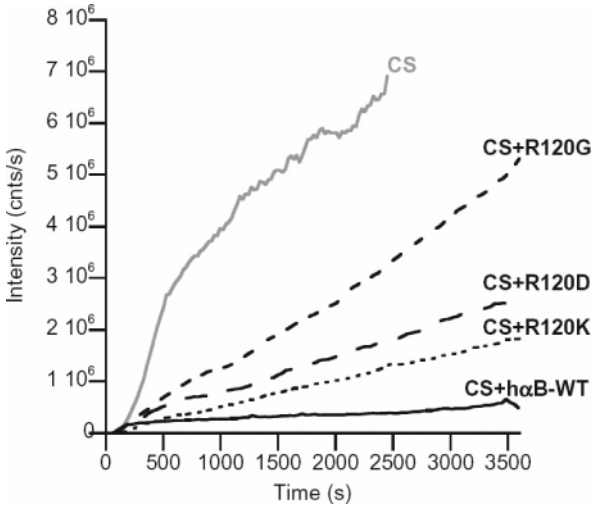

FIGURE 7: Chaperone-like activity of the αB-crystallin samples toward CS. Scattered intensity at 90° measured with the DLS instrument as a function of time at 48 °C. The CS and αB concentrations were ∼2.2 and ∼0.5 mg/mL, respectively. The CS/αB ratio was 4.5/1. The laser power sensitivity was 50%, and the acquisition time for one measurement was 10 s. Each experiment consisted of 180 or 360 measurements. Protection of CS provided by αB samples indicated the following: R120G < R120D < R120K < hαB-WT.

DISCUSSION

This study emphasizes the special role of residue 120 of αB-crystallin. Indeed, the observation that all the mutants that were studied, R120G, R120K, R120D, and R120C, behaved in a different way, both *in cellulo* and *in vitro*, was particularly striking. It was already established that, in mammalian cells, hαB-WT was mainly localized in the cytoplasm. Instead, the R120G mutant was known to result in the formation of cytoplasmic aggregates in a time-dependent process. First, multiple foci appear in the cytoplasm of transfected cells. Second, these multifocus-type aggregates are retrotransported along microtubules to form large peri-centrosomal masses (*34*). In the study presented here, we have transfected Cos-7 and NIH-3T3 cell lines to determine the localization of the hαB-WT and mutants species. We have observed that hαB-WT and the R120K mutant exhibited mainly a diffuse cytoplasmic localization in both cell lines. In constrast, the R120G, R120D, and R120C expression induced the growth of aggregates in both cell lines. The location of the aggregates was also cytoplasmic. For all the αB species, a few Cos-7 cells also displayed a nuclear immunostaining. To further characterize the ability to form aggregates of the different mutants, we have determined the number of transfected cells containing aggregates both 24 and 48 h after the transfection. Our results showed that hαB-WT and the R120K mutant remained soluble in the cytoplasm. In comparison, the R120G, R120D, and R120C mutants exhibited a significant level of transfected cells with aggregates 24 h post-transfection, which increased with time. The lack of solubility was presumably associated with an increased level of exposure of hydrophobic patches on the surface and, therefore, an increased tendency to associate and aggregate (*35*−*37*). Interestingly, the increase in the number of transfected cells with aggregates appeared to be slower for the R120D mutant than for the R120G or R120C mutant. This phenomenon was not

due to a difference in the expression level of the proteins. According to these results, whatever the modification of the Arg residue, the cytoplasmic localization in unstressed Cos-7 or NIH-3T3 cells of the different αB species was preserved. On the other hand, conservation of the charge seemed to be required to keep a sufficient solubility, which is able to ensure a uniform localization. Indeed, the modification of the charge always resulted in the formation of a significant amount of aggregates. In addition, the level of aggregates was a function of mutation type.

The results obtained in the mammalian transfected cells were consistent with the expression patterns of hαB-WT and of the different mutants in *E. coli*. hαB-WT and the R120K mutant were essentially in the soluble fraction; the R120G and R120D mutants were found in both soluble and insoluble fractions, whereas the R120C mutant was completely found in the insoluble fraction. Since the size and molecular mass of α-crystallin were known to be particularly sensitive to environmental conditions (*38*), no attempt was made to resolubilize the inclusion bodies, which precluded any further *in vitro* study of the R120C mutant.

The purification of the different αB species allowed us first to check the stability of the different αB species *in vitro*, when stored in a cold room, as assessed by their ability to remain in solution as a function of time. Whereas the hαB-WT properties remained unchanged for a couple of weeks, we were able to show that any kind of mutation of the R120 residue destabilized the αB structure. Our study demonstrated once more the specificity of the R120G mutation since, in agreement with previous work (*39*), the R120G mutant was found to be inherently unstable in solution. The R120K and R120D mutants had a stability intermediate between those of the WT and the R120G mutant. To avoid additional complexity, the *in vitro* experiments were conducted using fresh protein preparations. Usually, DLS measurements were taken immediately after purification, on the same day.

The most striking property of the α-crystallins is their dynamic oligomeric structure. Previous studies had established that the R120G mutation in hαB-WT led to an increase in the average size of the oligomeric structure (*39*−*42*) while keeping the secondary structure essentially unchanged (*40*). Similar results were obtained for the R116C mutation in αA (*43*−*45*). The FPLC, DLS, and EM measurements presented here indicate that, whatever the amino acid replacing the R120 residue, the mutation induced an increase in both the average molecular mass and the polydispersity of the oligomeric structure, according to the following order: WT < R120K < R120D < R120G.

The behavior in solution of hαB-WT and R120 mutants after purification can probably be considered to reflect the behavior in a cell of freshly synthesized particles. It is therefore interesting to note that the less soluble mutants that were, in solution, the most prone to forming large oligomers were those forming the largest aggregates in the transfected cells. In both cases, R120K was quite similar to the WT, R120G and R120C were the least soluble, and R120D was between the WT and the other mutants. The mutation destabilized the native structure and probably exposed an increased number of association sites with, as a consequence, an increase in the oligomeric size that, ultimately, led to aggregation and precipitation. Keeping the same charge, i.e., replacing Arg with Lys, seemed to be the least traumatic, yet not neutral, change, whereas a change in charge, i.e., the replacement of Arg with Asp, had severe consequences in terms of aggregation. However, the situation seemed much more complex than a simple electrostatic effect, since the stability appeared to be modified as well, with the less stable mutant being R120G. Finally, the R120C mutation, which seemed to be associated with a particularly low solubility, could correspond well to the exposure of a site particularly sensitive to oxidation, leading to the formation of aggregates through additional disulfide bonds. All these results suggest that the presence of an Arg residue at position 120 of αB is essential to conserve its oligomerization properties. These results are at variance with those obtained for hαA-WT in which the replacement of R116 with a residue bearing the same charge, R116K, was enough to essentially preserve the oligomeric size *in vitro* (*45*).

The α-crystallin chaperone-like activity was known to protect against stress through the binding of a variety of partially unfolded substrates, in a substrate-dependent manner (*24*, *25*, *29*, *46*−*49*). In some cases, an "activation" could be required; e.g., the active form of native calf α-crystallin toward γ-crystallins was an 80-mer as compared to the 40-mer of the native structure (*24*). Previous studies on the R120G mutant had shown a decrease in the chaperone-like activity associated with the increased oligomeric size and the decreased stability (*39*−*41*, *50*). Our study demonstrates that all the mutants presented quaternary structure modifications and were functionally impaired. In addition, the results obtained with the R120K mutant demonstrated that a modified quaternary structure may result in functional impairment even though sufficient solubility is retained to ensure a normal cytoplasmic location. The functional impairment varied in a substrate-dependent manner. In agreement with previous studies, the chaperone activity of the R120G mutant toward ADH was completely lost; in contrast, this study shows that the chaperone activity toward CS was only moderately reduced. Another novelty of our study was to show that, as far as the chaperone-like activity is concerned, all the mutants behaved in a similar way: none of them was able to prevent ADH aggregation, and all of them were providing some protection toward CS aggregation. In this context, it is interesting to note that the R120 residue is located in a region that had been identified as an interactive sequence for chaperone activity with ADH but not with CS (*48*). This might be the reason why mutations in the R120 region differently affect the chaperone activity toward the two target proteins.

Similarities between the pathological consequences of the R120G mutation in αB and of the R116C mutation in αA are well-known. Previous αA studies have demonstrated the conservation of a positive charge at this position was enough to preserve the functional properties of αA (*45*). Indeed, the replacement of the Arg residue with a Lys conserved the chaperone function assessed as the ability to suppress ADH aggregation. The study presented here demonstrates that preserving the charge at position 120 of αB was not sufficient to preserve its chaperone-like activity toward ADH and that, despite the high level of homology between αA and αB, these two proteins possess their own characteristics.

Taken together, all the results seemed to indicate a significant variability of the environment of the residue in position 120 from the WT to the different mutants, or from

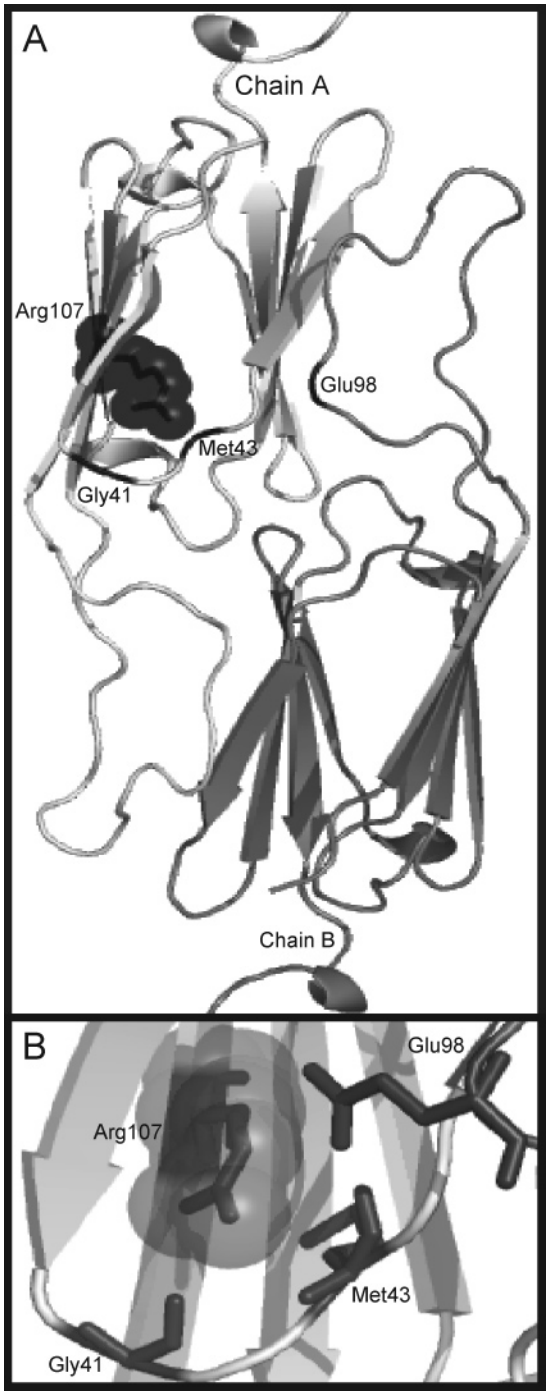

FIGURE 8: Representation of an α-crystallin domain dimer of HSP 16.5 (Protein Data Bank entry 1SHS). (A) Location of Arg-107 of HSP 16.5, which is equivalent to Arg-120 of hαB. (B) Local side chain interactions in the HSP 16.5 structure. Residues supposed to interact with Arg-107 of HSP 16.5 are reported. The analysis of the other published 3D structures also indicates interactions with residues located in neighboring loops.

one crystallin to another. In an attempt to visualize such an environment, the 3D structure of a subunit dimer of HSP 16.5 (Protein Data Bank entry 1SHS) was represented in Figure 8A,B. As one can see in the figure, the R107 residue in one subunit, equivalent to the R120 residue of αB, interacts with residues localized on neighboring loops: residues G41 and M43 on the loop which connects the β-strands 1 and 2 of the same subunit and residue E98 which is located on the large loop connecting the strands β5 and β7, yet from the other subunit. R107 could therefore be involved in the stability of the HSP 16.5 local dimeric structure. Since the loop regions are flexible and, moreover, the large loop is known to be especially variable from one species to the other, it therefore appears rational that a single mutation in such regions might modify a wide series of interactions and associations with a huge variability among species. The study advocates that the Arg residue at position 120 of αB plays a crucial role in the control of quaternary structure and interaction sites and is mandatory for hαB-WT quaternary structure integrity and function.

ACKNOWLEDGMENT

We gratefully acknowledge the help of Elodie Duprat for bioinformatics and structure display and of Céline Férard for molecular biology.

REFERENCES

1. Ingolia, T. D., and Craig, E. A. (1982) Four small *Drosophila* heat shock proteins are related to each other and to mammalian α-crystallin, *Proc. Natl. Acad. Sci. U.S.A. 79*, 2360−2364.
2. Haslbeck, M., Franzmann, T., Weinfurtner, D., and Buchner, J. (2005) Some like it hot: The structure and function of small heat-shock proteins, *Nat. Struct. Mol. Biol. 12*, 842−846.
3. Sun, Y., and MacRae, T. H. (2005) Small heat shock proteins: Molecular structure and chaperone function, *Cell. Mol. Life Sci. 62*, 2460−2476.
4. Fontaine, J. M., Rest, J. S., Welsh, M. J., and Benndorf, R. (2003) The sperm outer dense fiber protein is the 10th member of the superfamily of mammalian small stress proteins, *Cell Stress Chaperones 8*, 62−69.
5. Kappe, G., Franck, E., Verschuure, P., Boelens, W. C., Leunissen, J. A., and de Jong, W. W. (2003) The human genome encodes 10 α-crystallin-related small heat shock proteins: HspB1−10, *Cell Stress Chaperones 8*, 53−61.
6. Fontaine, J. M., Sun, X., Benndorf, R., and Welsh, M. J. (2005) Interactions of HSP22 (HSPB8) with HSP20, αB-crystallin, and HSPB3, *Biochem. Biophys. Res. Commun. 337*, 1006−1011.
7. Sugiyama, Y., Suzuki, A., Kishikawa, M., Akutsu, R., Hirose, T., Waye, M. M., Tsui, S. K., Yoshida, S., and Ohno, S. (2000) Muscle develops a specific form of small heat shock protein complex composed of MKBP/HSPB2 and HSPB3 during myogenic differentiation, *J. Biol. Chem. 275*, 1095−1104.
8. Sun, Y., and MacRae, T. H. (2005) The small heat shock proteins and their role in human disease, *FEBS J. 272*, 2613−2627.
9. Vicart, P., Caron, A., Guicheney, P., Li, Z., Prevost, M. C., Faure, A., Chateau, D., Chapon, F., Tome, F., Dupret, J. M., Paulin, D., and Fardeau, M. (1998) A missense mutation in the αB-crystallin chaperone gene causes a desmin-related myopathy, *Nat. Genet. 20*, 92−95.
10. Litt, M., Kramer, P., LaMorticella, D. M., Murphey, W., Lovrien, E. W., and Weleber, R. G. (1998) Autosomal dominant congenital cataract associated with a missense mutation in the human α crystallin gene CRYAA, *Hum. Mol. Genet. 7*, 471−474.
11. Irobi, J., Van Impe, K., Seeman, P., Jordanova, A., Dierick, I., Verpoorten, N., Michalik, A., De Vriendt, E., Jacobs, A., Van Gerwen, V., Vennekens, K., Mazanec, R., Tournev, I., Hilton-Jones, D., Talbot, K., Kremensky, I., Van Den Bosch, L., Robberecht, W., Van Vandekerckhove, J., Broeckhoven, C., Gettemans, J., De Jonghe, P., and Timmerman, V. (2004) Hot-spot residue in small heat-shock protein 22 causes distal motor neuropathy, *Nat. Genet. 36*, 597−601.
12. Zhang, F. F., Tang, B. S., Zhao, G. H., Chen, B., Zhang, C., Luo, W., Liu, X. M., Xia, K., Cai, F., Hu, Z. M., Yan, X. X., Zhang, R. X., and Guo, P. (2005) Mutation analysis of small heat-shock protein 22 gene in Chinese patients with Charcot-Marie-Tooth disease, *Zhonghua Yixue Yichuanxue Zazhi 22*, 361−363.
13. Chavez Zobel, A. T., Lambert, H., Theriault, J. R., and Landry, J. (2005) Structural instability caused by a mutation at a conserved arginine in the α-crystallin domain of Chinese hamster heat shock protein 27, *Cell Stress Chaperones 10*, 157−166.

14. de Jong, W. W., Caspers, G. J., and Leunissen, J. A. (1998) Genealogy of the α-crystallin−small heat-shock protein superfamily, *Int. J. Biol. Macromol. 22*, 151−162.
15. Bloemendal, H., de Jong, W., Jaenicke, R., Lubsen, N. H., Slingsby, C., and Tardieu, A. (2004) Ageing and vision: Structure, stability and function of lens crystallins, *Prog. Biophys. Mol. Biol. 86*, 407−485.
16. Aquilina, J. A., Benesch, J. L., Bateman, O. A., Slingsby, C., and Robinson, C. V. (2003) Polydispersity of a mammalian chaperone: Mass spectrometry reveals the population of oligomers in αB-crystallin, *Proc. Natl. Acad. Sci. U.S.A. 100*, 10611−10616.
17. Kim, K. K., Kim, R., and Kim, S. H. (1998) Crystal structure of a small heat-shock protein, *Nature 394*, 595−599.
18. van Montfort, R. L., Basha, E., Friedrich, K. L., Slingsby, C., and Vierling, E. (2001) Crystal structure and assembly of a eukaryotic small heat shock protein, *Nat. Struct. Biol. 8*, 1025−1030.
19. Stamler, R., Kappe, G., Boelens, W., and Slingsby, C. (2005) Wrapping the α-crystallin domain fold in a chaperone assembly, *J. Mol. Biol. 353*, 68−79.
20. Hilario, E., Teixeira, E. C., Pedroso, G. A., Bertolini, M. C., and Medrano, F. J. (2006) Crystallization and preliminary X-ray diffraction analysis of XAC1151, a small heat-shock protein from *Xanthomonas axonopodis* pv. citri belonging to the α-crystallin family, *Acta Crystallogr. F62*, 446−448.
21. White, H. E., Orlova, E. V., Chen, S., Wang, L., Ignatiou, A., Gowen, B., Stromer, T., Franzmann, T. M., Haslbeck, M., Buchner, J., and Saibil, H. R. (2006) Multiple distinct assemblies reveal conformational flexibility in the small heat shock protein Hsp26, *Structure 14*, 1197−1204.
22. Bova, M. P., Ding, L. L., Horwitz, J., and Fung, B. K. (1997) Subunit exchange of αA-crystallin, *J. Biol. Chem. 272*, 29511−29517.
23. Aquilina, J. A., Benesch, J. L., Ding, L. L., Yaron, O., Horwitz, J., and Robinson, C. V. (2005) Subunit exchange of polydisperse proteins: Mass spectrometry reveals consequences of αA-crystallin truncation, *J. Biol. Chem. 280*, 14485−14491.
24. Putilina, T., Skouri-Panet, F., Prat, K., Lubsen, N. H., and Tardieu, A. (2003) Subunit exchange demonstrates a differential chaperone activity of calf α-crystallin toward *β*LOW- and individual *γ*-crystallins, *J. Biol. Chem. 278*, 13747−13756.
25. Horwitz, J. (1992) α-Crystallin can function as a molecular chaperone, *Proc. Natl. Acad. Sci. U.S.A. 89*, 10449−10453.
26. Basha, E., Lee, G. J., Demeler, B., and Vierling, E. (2004) Chaperone activity of cytosolic small heat shock proteins from wheat, *Eur. J. Biochem. 271*, 1426−1436.
27. Ghosh, J. G., and Clark, J. I. (2005) Insights into the domains required for dimerization and assembly of human αB crystallin, *Protein Sci. 14*, 684−695.
28. Shashidharamurthy, R., Koteiche, H. A., Dong, J., and McHaourab, H. S. (2005) Mechanism of chaperone function in small heat shock proteins: Dissociation of the HSP27 oligomer is required for recognition and binding of destabilized T4 lysozyme, *J. Biol. Chem. 280*, 5281−5289.
29. Bhattacharyya, J., Padmanabha Udupa, E. G., Wang, J., and Sharma, K. K. (2006) Mini-αB-crystallin: A functional element of αB-crystallin with chaperone-like activity, *Biochemistry 45*, 3069−3076.
30. Ghosh, J. G., Shenoy, A. K., Jr., and Clark, J. I. (2006) N- and C-terminal motifs in human αB crystallin play an important role in the recognition, selection, and solubilization of substrates, *Biochemistry 45*, 13847−13854.
31. Rajan, S., Horn, C., and Abraham, E. C. (2006) Effect of oxidation of αA- and αB-crystallins on their structure, oligomerization and chaperone function, *Mol. Cell. Biochem. 288*, 125−134.
32. Mehlen, P., Hickey, E., Weber, L. A., and Arrigo, A. P. (1997) Large unphosphorylated aggregates as the active form of hsp27 which controls intracellular reactive oxygen species and glutathione levels and generates a protection against TNFα in NIH-3T3-ras cells, *Biochem. Biophys. Res. Commun. 241*, 187−192.
33. Skouri-Panet, F., Quevillon-Cheruel, S., Michiel, M., Tardieu, A., and Finet, S. (2006) sHSPs under temperature and pressure: The opposite behaviour of lens α-crystallins and yeast HSP26, *Biochim. Biophys. Acta* (in press).
34. Chavez Zobel, A. T., Loranger, A., Marceau, N., Theriault, J. R., Lambert, H., and Landry, J. (2003) Distinct chaperone mechanisms can delay the formation of aggresomes by the myopathy-causing R120G αB-crystallin mutant, *Hum. Mol. Genet. 12*, 1609−1620.
35. Bhattacharyya, J., Srinivas, V., and Sharma, K. K. (2002) Evaluation of hydrophobicity versus chaperonelike activity of bovine αA- and αB-crystallin, *J. Protein Chem. 21*, 65−71.
36. Srinivas, V., Raman, B., Rao, K. S., Ramakrishna, T., and Rao, Ch. M. (2003) Structural perturbation and enhancement of the chaperone-like activity of α-crystallin by arginine hydrochloride, *Protein Sci. 12*, 1262−1270.
37. Reddy, G. B., Kumar, P. A., and Kumar, M. S. (2006) Chaperone-like activity and hydrophobicity of α-crystallin, *IUBMB Life 58*, 632−641.
38. Tardieu, A., Laporte, D., Licinio, P., Krop, B., and Delaye, M. (1986) Calf lens α-crystallin quaternary structure. A three-layer tetrahedral model, *J. Mol. Biol. 192*, 711−724.
39. Treweek, T. M., Rekas, A., Lindner, R. A., Walker, M. J., Aquilina, J. A., Robinson, C. V., Horwitz, J., Perng, M. D., Quinlan, R. A., and Carver, J. A. (2005) R120G αB-crystallin promotes the unfolding of reduced α-lactalbumin and is inherently unstable, *FEBS J. 272*, 711−724.
40. Bova, M. P., Yaron, O., Huang, Q., Ding, L., Haley, D. A., Stewart, P. L., and Horwitz, J. (1999) Mutation R120G in αB-crystallin, which is linked to a desmin-related myopathy, results in an irregular structure and defective chaperone-like function, *Proc. Natl. Acad. Sci. U.S.A. 96*, 6137−6142.
41. Kumar, L. V., Ramakrishna, T., and Rao, C. M. (1999) Structural and functional consequences of the mutation of a conserved arginine residue in αA and αB crystallins, *J. Biol. Chem. 274*, 24137−24141.
42. Cobb, B. A., and Petrash, J. M. (2000) Structural and functional changes in the αA-crystallin R116C mutant in hereditary cataracts, *Biochemistry 39*, 15791−15798.
43. Shroff, N. P., Cherian-Shaw, M., Bera, S., and Abraham, E. C. (2000) Mutation of R116C results in highly oligomerized αA-crystallin with modified structure and defective chaperone-like function, *Biochemistry 39*, 1420−1426.
44. Bera, S., and Abraham, E. C. (2002) The αA-crystallin R116C mutant has a higher affinity for forming heteroaggregates with αB-crystallin, *Biochemistry 41*, 297−305.
45. Bera, S., Thampi, P., Cho, W. J., and Abraham, E. C. (2002) A positive charge preservation at position 116 of αA-crystallin is critical for its structural and functional integrity, *Biochemistry 41*, 12421−12426.
46. Santhoshkumar, P., and Sharma, K. K. (2001) Analysis of α-crystallin chaperone function using restriction enzymes and citrate synthase, *Mol. Vision 7*, 172−177.
47. Horwitz, J. (2003) α-Crystallin, *Exp. Eye Res. 76*, 145−153.
48. Ghosh, J. G., Estrada, M. R., and Clark, J. I. (2005) Interactive domains for chaperone activity in the small heat shock protein, human αB crystallin, *Biochemistry 44*, 14854−14869.
49. Ecroyd, H., Meehan, S., Horwitz, J., Aquilina, J. A., Benesch, J. L., Robinson, C. V., Macphee, C. E., and Carver, J. A. (2007) Mimicking phosphorylation of αB-crystallin affects its chaperone activity, *Biochem. J. 401*, 129−141.
50. Perng, M. D., Muchowski, P. J., van Den, I. P., Wu, G. J., Hutcheson, A. M., Clark, J. I., and Quinlan, R. A. (1999) The cardiomyopathy and lens cataract mutation in αB-crystallin alters its protein structure, chaperone activity, and interaction with intermediate filaments in vitro, *J. Biol. Chem. 274*, 33235−33243.

BI7003125